Atmospheric Environment 320 (2024) 120339

Contents lists available at ScienceDirect

Atmospheric Environment

journal homepage: www.elsevier.com/locate/atmosenv

Assessing the impact of shipping emissions on ozone concentrations in East Asia: Insights from KORUS-AQ and SIJAQ 2021 campaign periods

Jaehyeong Park [a], Jeonghyeok Mun [a,b], Dongjin Kim [a,b], Hwa Woon Lee [c], Cheol-Hee Kim [b,c], Hyo-Jung Lee [b,c], Hyun-Young Jo [d], Ja-Yong Koo [e], Hyeonsik Choe [a,b], Wonbae Jeon [b,c,*]

[a] Division of Earth Environmental System, Pusan National University, Busan, 46241, South Korea
[b] BK21 School of Earth and Environmental System, Pusan National University, Busan, 46241, South Korea
[c] Department of Atmospheric Sciences, Pusan National University, Busan, 46241, South Korea
[d] Institute of Environmental Studies, Pusan National University, Busan, 46241, South Korea
[e] WIZAI Co., Ltd., Seoul, 08590, South Korea

HIGHLIGHTS

- O_3 concentration changes in the East Asian regions due to ocean emissions during the KORUS-AQ and SIJAQ campaign periods are investigated.
- The influence of ocean emissions on the production and loss of O_3 varies by region and season.
- The ocean emissions could result in the transition of the O_3 sensitivity regime in some ocean areas.
- The seasonal transport of ocean emissions to BVOC-rich inland regions can contribute to the increase in O_3 concentration.

GRAPHICAL ABSTRACT

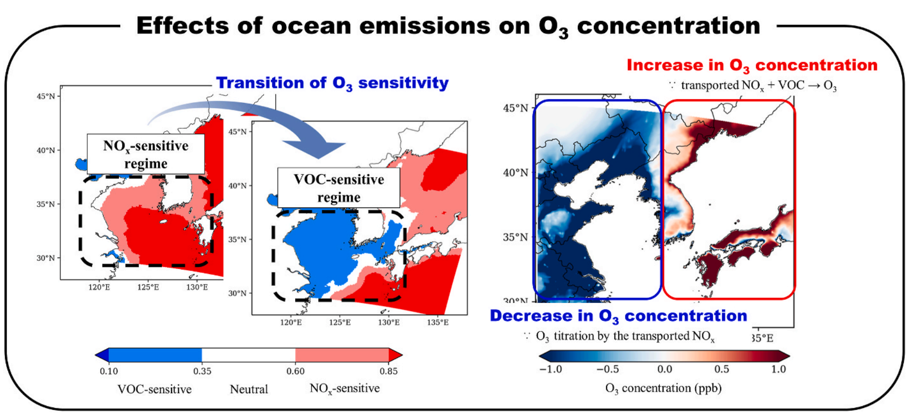

ARTICLE INFO

Keywords:
KORUS-AQ
SIJAQ campaign
CMAQ
O_3
Shipping emissions

ABSTRACT

This study analyzed the impact of shipping emissions on ozone (O_3) concentrations in East Asia during the Korea-United States Air Quality (KORUS-AQ) and the Satellite Integrated Joint monitoring for Air Quality (SIJAQ) 2021 campaign period. Numerical simulations were performed during the KORUS-AQ (May 2016, the KORUS case) and the SIJAQ 2021 (October–November 2021, the SIJAQ case) using Community Multi-scale Air Quality (CMAQ), the three-dimensional chemical transport model. We additionally simulated an experiment without shipping emissions to compare the impact with and without shipping emissions. Using the validated simulation results, the average O_3 concentrations in inland regions were found to be 35.63 ppb and 20.62 ppb in the KORUS and SIJAQ cases, respectively. The average O_3 concentrations were higher in the KORUS case owing to the difference in weather conditions between the two cases in various seasons. The results of examining the impact of shipping emissions on O_3 concentrations in the ocean area indicate that both the KORUS and SIJAQ cases resulted in a decrease in O_3 concentrations in the Yellow Sea region, while the O_3 concentrations increased in the

* Corresponding author. BK21 School of Earth and Environmental System, Pusan National University, Busan, 46241, South Korea.
E-mail address: wbjeon@pusan.ac.kr (W. Jeon).

https://doi.org/10.1016/j.atmosenv.2024.120339
Received 11 June 2023; Received in revised form 7 December 2023; Accepted 6 January 2024
Available online 8 January 2024
1352-2310/

East Sea and North Pacific regions. In particular, in the Yellow Sea and East China Sea, where the O_3 concentrations decreased in the KORUS case, O_3 sensitivity results showed volatile organic compounds (VOC)-sensitive regime when the shipping emissions were removed but changed to nitrogen oxide (NO_x)-sensitive regime when the shipping emissions were added. Meanwhile, in the inland regions, the SIJAQ case decreased O_3 concentrations in most areas, whereas the KORUS case showed an increase in O_3 concentrations in the Korean Peninsula and Japan. Analysis of O_3 sensitivity revealed that the regions of the Korean Peninsula and Japan, where O_3 concentrations increased, exhibited a NO_x-sensitive regime. Particularly, in the case of the Korean Peninsula, the initial transport of shipping emissions in the western part led to a decrease in O_3 concentrations. However, as shipping emissions were further transported from west to east, they became more diluted, and additional NO_x generated by O_3 titration reactions was also transported, gradually increasing O_3 concentrations. Furthermore, we found that during seasons with abundant BVOC emissions, the transport of shipping emissions could contribute to additional O_3 production. These results confirmed that shipping emissions in East Asia primarily reduce O_3 concentrations, however, differences in seasonal and regional O_3 sensitivity and transportation patterns can contribute to O_3 production.

1. Introduction

East Asia has reported the largest growth in anthropogenic emissions worldwide owing to rapid industrial growth over the past few decades (Jung et al., 2022; Lee et al., 2019; Singh et al., 2021). Countries in East Asia have been endeavoring to reduce the concentrations of pollutants through national O_3 reduction plans and emissions reduction, among other strategies (Lee and Woo, 2020; Lin and Zhu, 2019; Qi et al., 2022; Sugiyama et al., 2019; Xu et al., 2019). Nevertheless, O_3 concentrations show an increasing trend (Chang et al., 2017; Takahashi et al., 2020), and among East Asian countries, O_3 concentrations in China and South Korea are increasing rapidly (Kim et al., 2018; Lee et al., 2020; Mun et al., 2023). In particular, the concentrations of O_3 vary depending on the emissions of precursors and atmospheric conditions. Therefore, exploring the processes of O_3 production and destruction is crucial for the implementation of policies to reduce the negative effects of O_3.

In recent times, several studies have been conducted to investigate the factors contributing to this increase in O_3 concentrations in East Asia. T. Wang et al. (2019) analyzed the long-term trends of O_3 in East Asia as a function of emissions and meteorological patterns over 25 years. Itahashi et al. (2022) used satellite-measured column densities of formaldehyde (HCHO) and nitrogen dioxide (NO_2) to diagnose the sensitivity of O_3 in East Asian countries. Lee et al. (2022) examined the O_3 formation regime across nine megacities in East Asia using O_3 columns, NO_2, and HCHO from measurements by ozone-monitoring instruments (OMI). Song et al. (2022) used the summer daily meteorological data and surface O_3 concentrations of the Coupled Model Intercomparison Project Phase 6 (CMIP6) to investigate changes in O_3 concentrations under synoptic climate types. Furthermore, the National Institute of Environmental Research (NIER) in South Korea, in collaboration with the National Aeronautics and Space Administration (NASA), conducted the Korea-United States Air Quality (KORUS-AQ) field study from May to mid-June to identify the main controlling factors of O_3 produced in South Korea (Choi et al., 2019; Crawford et al., 2021; Peterson et al., 2019).

In addition, the Satellite Integrated Joint Monitoring for Air Quality (SIJAQ) is being conducted for the second phase to compensate for the short study period of KORUS-AQ and try to identify the causes of increasing O_3 concentrations in the East Asian region. However, owing to the nature of O_3, which can be produced from various sources, more detailed research is needed to understand the production and dissipation of O_3.

Emission sources that affect O_3 production and dissipation can be broadly categorized as inland and ocean. Of these, ocean sources can be divided into natural sources that emit directly from the ocean and anthropogenic sources, such as emissions from the movement and anchoring of ships. The East Asian region is densely populated with countries adjacent to the sea. Over the course of several decades, ocean trade has experienced significant growth, leading to continuous development in shipping and ports. Consequently, this region has been witnessing an increasing discharge of anthropogenic pollutants into the ocean. According to the 2022 Review of Ocean Transport (UNCTAD, 2022), the Asia region accounts for 42% of global exports and 64% of global imports in world ocean trade. Furthermore, it holds a significant

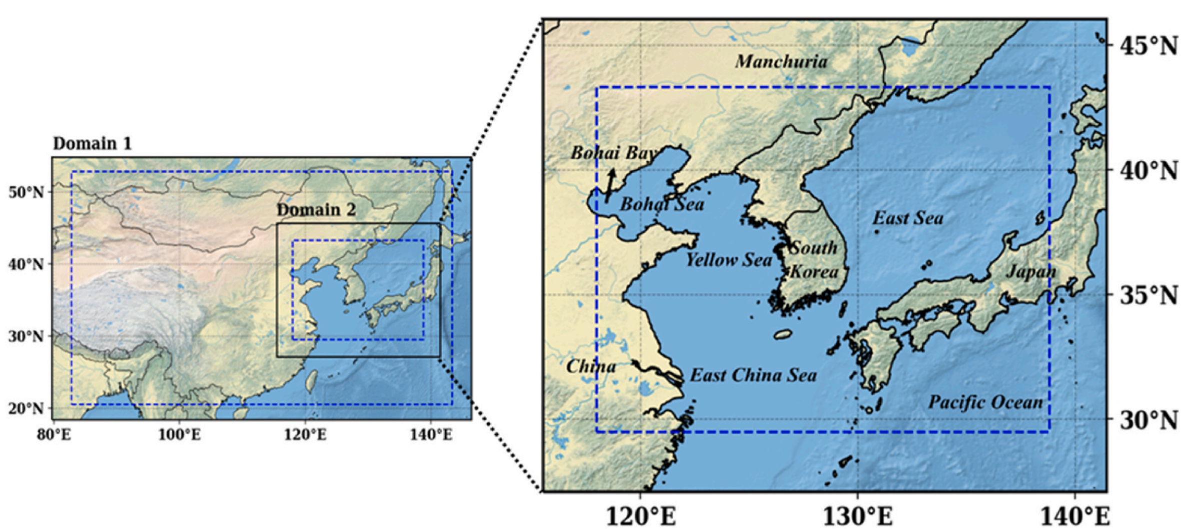

Fig. 1. Left panel shows the domains for Weather Research and Forecasting (WRF) and Community Multi-scale Air Quality (CMAQ) numerical simulations. In the left panel, the blue box represents the CMAQ domains, and the black box represents the WRF domains. The right panel is Domain 2 and includes detailed nominations for the analysis of O_3 concentrations caused by shipping emissions.

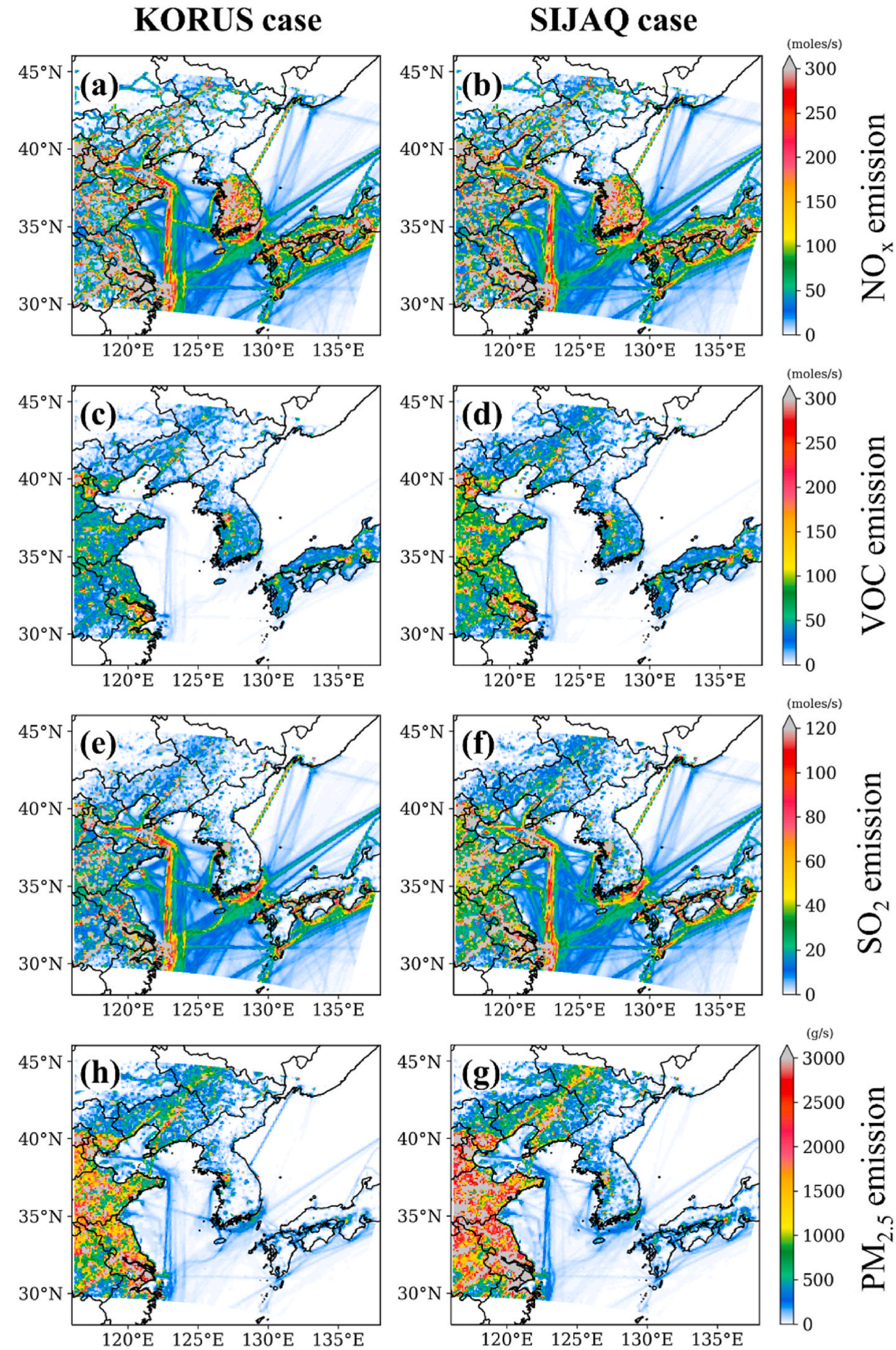

Fig. 2. Spatial distribution of EDGARv6.1 emission in the analysis area during the analysis periods of the KORUS case (left) and SIJAQ case (right). Emissions over the analysis period were summed up, and substances represent NO_x ((a) and (b)), VOC ((c) and (d)), SO_2 ((e) and (f)), and $PM_{2.5}$ ((g) and (h)).

share of 64.3% in cargo loading and handling, and the volume of international ship movements continues to increase annually. Ships emit pollutants such as carbon monoxide (CO), methane (CH_4), black carbon (BC), sulfur dioxide (SO_2), nitrogen oxide (NO_x), and non-methane volatile organic compounds (NMVOC) (EEA and EMSA, 2021). NO_x and NMVOC are the main precursors to O_3 formation, and O_3 produced from ocean sources can affect neighboring countries.

Therefore, this study examined the impact of shipping emissions on O_3 concentrations during the KORUS-AQ, a field study on air quality in South Korea, one of the countries in East Asia, and the SIJAQ 2021 campaign, a follow-up study to the KORUS-AQ. The shipping emissions data from EDGARv6.1, an anthropogenic emissions dataset used in the air quality numerical model, were utilized to simulate O_3 concentrations in East Asia for each case. Furthermore, we analyzed the changes in O_3 concentrations attributed to shipping emissions for both inland and ocean regions during each period.

2. Methodology

2.1. Overview of the study area

East Asia, the target region of this study, is a mid-latitude region located in the eastern part of the Asian continent and includes countries such as China, South Korea, and Japan, as shown in Fig. 1. This region is

Table 1
The total amount of EDGARv6.1 emission (Total) and the total amount of shipping emissions (Shipping) during the KORUS case in Domain 2. Shipping/Total indicates the percentage of shipping emissions in total emissions.

	CO	BC	OC	SO_2	NO_x	NH_3	NMVOC	PM_{10}	$PM_{2.5}$
Total (10^{-11}kg/m^2/s)	175,678	1497	3125	55,712	43,483	8133	37,162	23,558	16,821
Shipping (10^{-11}kg/m^2/s)	7263	143	155	6903	7959	206	3772	1580	1247
Shipping/Total (%)	4.13	9.54	4.96	12.39	18.30	2.53	10.15	6.71	7.41

influenced by both continental and ocean climates and characterized by hot and humid weather in summer and cold and dry weather in winter. Moreover, long-distance transportation between countries is frequent owing to the monsoon zone (Griffith et al., 2020; Li et al., 2016; Shimadera et al., 2013; Uranishi et al., 2019; Vogel et al., 2016; Wang et al., 2016). In this region, various pollutants are emitted from industrial areas and ports located along the coasts of the Pacific Ocean, South China Sea, Yellow Sea, and East Sea, as well as from ships traveling to these ports (Ducruet et al., 2010; Wang et al., 2010, 2014). Furthermore, approximately half of the area constitutes boreal forests, and other vegetation, such as cropland and grassland, account for approximately 30% of the area (Fu et al., 2022; Luo et al., 2020). Therefore, the complex chemical processes of anthropogenic and natural emissions cause various air quality pollution phenomena.

2.2. Study period

In 2016, NIER and NASA measured air pollutants in South Korea, including fine particulate matter ($PM_{2.5}$), through the KORUS-AQ from May to mid-June and performed air quality model analyses to identify key controlling factors of $PM_{2.5}$ and O_3. KORUS-AQ measured the atmospheric composition of the Korean Peninsula and surrounding shore regions to analyze the factors contributing to the deterioration of air quality in South Korea and sampled various data from multiple airborne and ground-based remote sensing and in situ measurements to evaluate air quality forecast results. Although KORUS-AQ provided measurements over an extensive area, both horizontally and vertically, the study period was insufficient to describe the air quality problems in South Korea. For this reason, to complement KORUS-AQ and further enhance the study of atmospheric pollution in the Korean Peninsula and Asia, a second phase of international collaborative research on air quality, known as the SIJAQ campaign, is planned to 2024. This initiative aims to validate the Geostationary Environment Monitoring Spectrometer (GEMS), South Korea's geostationary environmental satellite, while conducting research on atmospheric pollution in South Korea and the surrounding region. In response, 25 research teams from NIER, NASA, and other organizations in South Korea carried out the SIJAQ 2021 campaign from October 18 to November 26, 2021, to understand the distribution of air pollutants in the South Korean metropolitan area. The SIJAQ 2021 campaign aimed to identify the formation process of $PM_{2.5}$ in urban areas (particularly nitrate and organic aerosol formation) by using ground observation equipment to observe air pollutants in the metropolitan area of South Korea in three dimensions and to improve the reliability of O_3 observation data by GEMS, ultimately preparing measures to control $PM_{2.5}$ and O_3 pollution.

In this study, we analyzed the impact of shipping emissions on O_3 concentrations for the aforementioned KORUS-AQ and SIJAQ 2021 campaign periods. To this end, we simulated the KORUS-AQ period (May 2016, the KORUS case) and the SIJAQ 2021 period (October–November 2021, the SIJAQ case) with and without shipping emissions, respectively. We then analyzed the O_3 concentrations in each modeling period to determine the impact of shipping emissions on O_3 concentrations in the East Asian region during the KORUS-AQ and SIJAQ 2021 campaign periods.

2.3. Modeling system

Air quality numerical simulations were performed to analyze the O_3 concentrations in the KORUS and SIJAQ cases, considering the differences in shipping emissions. The numerical air quality simulation utilized Community Multi-scale Air Quality (CMAQ, v5.3.2, Ching and Byun, 1999; Appel et al., 2021), a three-dimensional photochemical model developed by the U.S. Environmental Protection Agency (EPA). Weather Research and Forecasting (WRF, v4.1.1, Skamarock et al., 2019) was used to generate meteorological inputs for the CMAQ simulation. The numerical simulation domain utilized observations during the KORUS and SIJAQ cases. Domain 1 (D1, 165 × 129), with a resolution of 27 km, including China, South Korea, and Japan, and Domain 2 (D2, 213 × 186), with a resolution of 9 km, were established to analyze the phenomenon more comprehensively using the results of D1 as initial and boundary fields of accounting for the effects of long-range transport and shipping emissions between countries (Fig. 1). The vertical grid has 15 layers, with the top layer set to 100 hPa. Grid nudging was utilized to improve the accuracy of meteorological numerical simulation results used as input for air quality models (Jeon et al., 2015; Stauffer and Seaman, 1990; Vincent and Hahmann, 2015). The detailed settings utilized in the meteorological and air quality numerical simulations are shown in Tables S1 and S2, respectively. Among the simulated results, the KORUS case was used for the analysis from May 1, 2016, 00UTC to June 1, 2016, 00UTC, and the SIJAQ case was used from October 20, 2020, 00UTC to November 21, 2020, 00UTC.

2.4. Emissions

The anthropogenic emissions utilized in the air quality simulations were obtained from the Emission Database for Global Atmospheric Research (EDGAR, version 6.1, Crippa et al., 2022), a global emissions database. EDGARv6.1 emission has a horizontal resolution of 0.1° × 0.1°. It provides yearly emissions from 1970 to 2018 for $PM_{2.5}$, PM_{10}, SO_2, NO_x, CO, NMVOC, BC, OC, and NH_3. It also provides vertical and temporal (monthly, weekly, hourly) profiles for 25 sectors, including agriculture, aviation, power industry, and combustion, to produce emissions required for air quality models according to regional characteristics. Among the air quality numerical modeling cases conducted in this study, the KORUS case utilized EDGAR emission data for 2016. The SIJAQ case, which simulated the year 2021, utilized the most recently available EDGAR emission data for 2018. Fig. 2 shows the distribution of EDGAR emission data calculated in the D2 area during the analysis

Table 2
Same as Table 1, but for the SIJAQ case.

	CO	BC	OC	SO_2	NO_x	NH_3	NMVOC	PM_{10}	$PM_{2.5}$
Total (10^{-11}kg/m^2/s)	175,006	1465	3009	55,935	43,743	7608	37,335	23,456	16,662
Shipping (10^{-11}kg/m^2/s)	7045	148	155	7038	8187	203	3809	1632	1286
Shipping/Total (%)	4.03	10.07	5.14	12.58	18.72	2.66	10.20	6.96	7.72

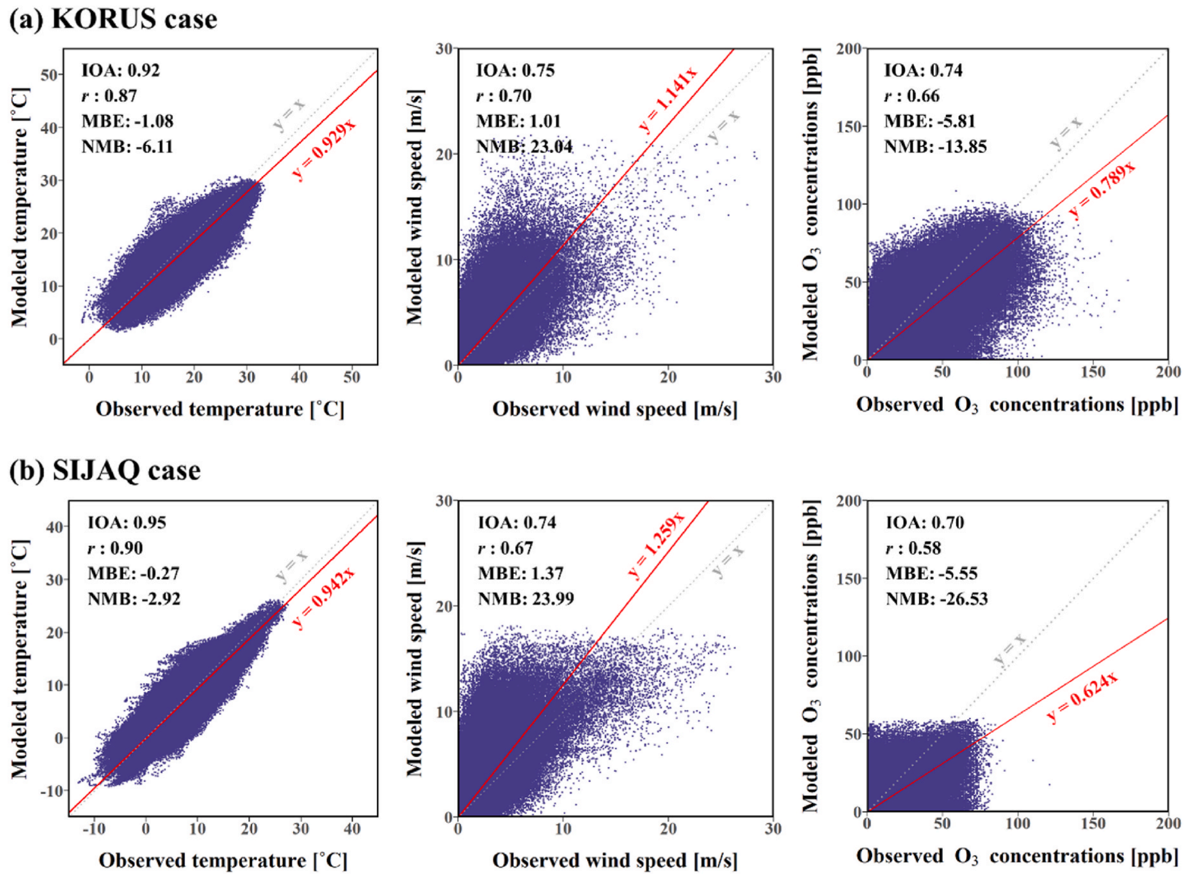

Fig. 3. Comparison of simulated results from WRF and CMAQ with observations of (a) the KORUS case and (b) the SIJAQ case. Scatterplots for air temperature are on the left, wind speed in the center, and O_3 concentrations are on the right, with the values of statistical parameters (IOA, *r*, MBE, and NMB) shown in each scatterplot.

period of the KORUS and SIJAQ cases, indicating that NO_x, SO_2, VOC, and $PM_{2.5}$ are mainly emitted from megacities, ports, and shipping lanes. Tables 1 and 2 show the total amount of NO_x and NMVOC, which are the main precursors of O_3, in the total amount of emissions for each case during the analysis period. They showed that the shipping emissions of NO_x and NMVOC in the KORUS case were 18.30% and 10.15% of the total emissions, respectively, and those in the SIJAQ case were 18.72% and 10.20% of the total emissions, respectively. These findings indicate that the proportion of pollutants emitted from the ocean to the total emissions in both cases was similar.

In addition, in the East Asian region, approximately 70% of the land area in South Korea is forested (Song and Park, 2021), and more than 60% of the land area is forested in North Korea and Japan (Morisada et al., 2004; Oh and Park, 2023). Biogenic emissions were considered because O3 is highly influenced by biogenic volatile organic compounds (BVOC) emitted from trees (Calfapietra et al., 2013; Liu et al., 2018). Biogenic emissions were simulated using the Model of Emissions of Gases and Aerosols from Nature v2.1 (MEGANv2.1, Guenther et al., 2012) for isoprene, monoterpenes, and other substances that make up a large proportion of BVOC.

2.5. Aircraft measurements

To evaluate the results of the air quality numerical model in three dimensions, we utilized flight observations conducted during the KORUS-AQ and SIJAQ 2021 campaign periods (Figs. S1 and S2). The KORUS-AQ field study conducted 20 flight observations (total flight time of approximately 150 h) in conjunction with the NASA DC-8 airborne research laboratory to identify the factors affecting air quality deterioration in South Korea (LeBlanc et al., 2022; Park et al., 2020). NASA's DC-8 conducted flight observations over the Korean Peninsula and surrounding shore regions. Through the observations of the main meteorological periods (i.e., "dynamic", "stagnation", "extreme pollution", and "blocking") that occurred during the study period, the air quality in South Korea was observed and quantified. In the case of SIJAQ 2021, 15 flight observations centered on the Seoul metropolitan area and the Yellow Sea coast were conducted (approximately 41 h of flight time) to elucidate the distribution of air pollutant concentrations in the South Korean metropolitan area. An imaging sensor with hyperspectral resolution developed by NASA was mounted on the aircraft to observe 11 types of air pollutants, including VOC, NH_3, NO_x, SO_2, CO, $PM_{2.5}$, and O_3, as well as meteorological factors such as temperature, humidity, and wind speed.

3. Results and discussion

3.1. Model performance evaluation

3.1.1. Evaluation of weather and air quality simulations based on ground observations

Before utilizing the results of the numerical simulation, we performed the simulated results, which were quantitatively verified to ensure their suitability for the analysis of the phenomenon. The observation data used for the verification were obtained from 257 weather stations of the Korea Meteorological Administration (KMA) in South Korea and 583 air quality monitoring stations of the NIER. The temperature, wind speed, and O_3 concentrations observations were used to verify the weather and air quality numerical model data. To quantitatively evaluate the results of the numerical model, we used the statistical indices used in previous studies: the index of agreement (IOA), the

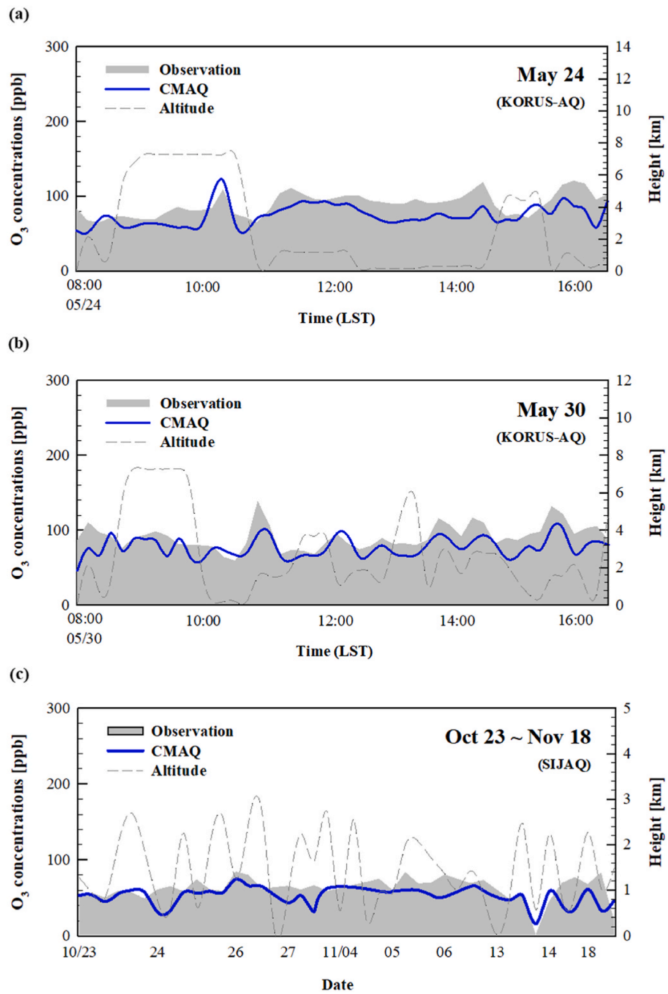

Fig. 4. Time series of O_3 concentrations (gray shading) measured through flight observations. (a) and (b) represent the O_3 concentrations values measured on May 24 and 30 during the KORUS-AQ period, respectively, while (c) represents the O_3 concentrations measured during the entire SIJAQ 2021 campaign period. The solid blue line represents the time series of O_3 concentrations simulated by CMAQ, and the gray dashed line indicates the altitude of the aircraft corresponding to the observation time.

correlation coefficient (*r*), the mean bias error (MBE), and the normalized mean bias (NMB). The formulas for the statistical indices used are presented in Table S4. The *r* represents the amount of agreement between predicted and observed variability (Emery et al., 2017), the IOA describes the error and concordance of the variability between model and observation, and the MBE and NMB indicate the quantitative errors. (Kim et al., 2022). According to previous studies, when evaluating simulation of accuracy, model results adequately describe the phenomenon if the *r* is > 0.5, the NMB is ±30% (Emery et al., 2017), and the IOA is > 0.5 (Willmott et al., 1985; Hurley et al., 2001), the performance is considered to be excellent if the *r* is > 0.75 and the NMB is within ±15% (Emery et al., 2017). The respective IOA values of air temperature, wind speed, and O_3 in the KORUS case were confirmed to be 0.949, 0.736, and 0.701; the *r* values were 0.87, 0.70, and 0.66; the MBE values were −0.272, 1.368, and −5.553, and the NMB values were −2.92, 23.99, and −26.53. The SIJAQ case yielded IOA values of 0.92, 0.75, and 0.74, *r* values of 0.90, 0.67, and 0.58, MBE values of 1.08, 1.01, and −5.83, and NMB values of −6.11, 23.04, and −13.85 (Fig. 3) for air temperature, wind speed, and O_3, respectively. In both cases, temperature and O_3 concentrations were underestimated, and wind speed was overestimated. However, the results of each numerical model met the reference values according to the accuracy evaluation results presented in previous studies.

3.1.2. Evaluation of air quality simulation based on aircraft measurement data

Using the O_3 concentrations of the KORUS and SIJAQ cases simulated by CMAQ and the aircraft measurements mentioned in Section 2.5, the variability of O_3 concentrations with time and altitude changes was checked in three dimensions. As shown in Fig. S1, during the KORUS case, on May 24 (Fig. 4(a)), an aircraft flew over the Yellow Sea coastal area, and on May 30 (Fig. 4(b)), an aircraft flew over the inland area and south coast of the Korean Peninsula. O_3 concentrations were observed for altitudes ranging from <100 m to 8 km. Comparing the flight observations with the numerical simulations, the KORUS case period generally underestimated O_3 concentrations. However, the variability of O_3 concentrations during the observation period was adequately simulated.

As shown in Fig. S2, the SIJAQ case flew over the metropolitan area of South Korea and parts of the Yellow Sea and observed O_3 concentrations up to a maximum altitude of 3 km, which is slightly lower than the KORUS case. Comparing the simulation results of the SIJAQ case with the flight observations (Fig. 4(c)), similar to the numerical simulation results of the KORUS case, the O_3 concentrations were underestimated. In particular, the O_3 concentrations were underestimated during decreasing altitudes (October 24, October 27, November 14, November 18); however, most of the simulation results of the O_3 concentrations considering time and altitude changes, including a sharp decrease in O_3 concentrations on November 13, were accurate.

The results of the vertical validation indicate that both cases slightly underestimated the O_3 concentrations, but the observed and simulated O_3 concentrations patterns are considerably similar. Therefore, based on the validation of the ground observations and flight observations, it was determined that the numerical simulation results are sufficient to explain the phenomenon.

3.2. Horizontal O_3 concentrations distribution characteristics for the KORUS and SIJAQ cases

Using the validated simulation results, the hourly average O_3 concentration distributions of the KORUS and SIJAQ cases were examined. First, the O_3 concentrations in the inland regions of the SIJAQ case, both in Fig. 5(a) with shipping emissions and in Fig. 5(b) without shipping emissions, were low in the South Korea and East China regions with high NO_x emissions compared to the Japan and North Korea regions with low NO_x emissions. The distributions of O_3 concentrations in the ocean regions were similar regardless of shipping emissions, with a somewhat lower O_3 concentration distribution in the Bohai Sea region. This is because pollutants emitted from an adjacent area to the Bohai Sea were transported to the Bohai Sea, and NO_x in the transported substances contributed to the O_3 titration reaction ($NO + O_3 \rightarrow NO_2 + O_2$, Jiménez et al., 2005; Akimoto et al., 2015), resulting in lower O_3 concentrations compared to other ocean areas (Fig. 5(c)).

In contrast, the O_3 concentrations in the KORUS case (Fig. 5(d) and (e)) were higher on average compared to the SIJAQ case, despite the high NO_x emissions. The average inland O_3 concentrations in the KORUS case were 35.63 ppb, thereby exceeding the average inland O_3 concentrations of 20.62 ppb in the SIJAQ case. This is attributed to the difference between the simulation period in the KORUS case, which is a period of high monthly average O_3 concentrations, and the simulation period in the SIJAQ case, which is a period of low monthly average O_3 concentrations (Zhao et al., 2015). Meteorological conditions were different between these two cases (relatively high temperature and intense insolation in the KORUS case), resulting in higher average O_3 concentrations in the KORUS case (Paraschiv et al., 2020; J. Wang et al., 2019). In the ocean regions, when considering shipping emissions, O_3 concentrations in the Bohai Sea and East China Sea noticeably decreased. This is because one of the largest port clusters in the world is

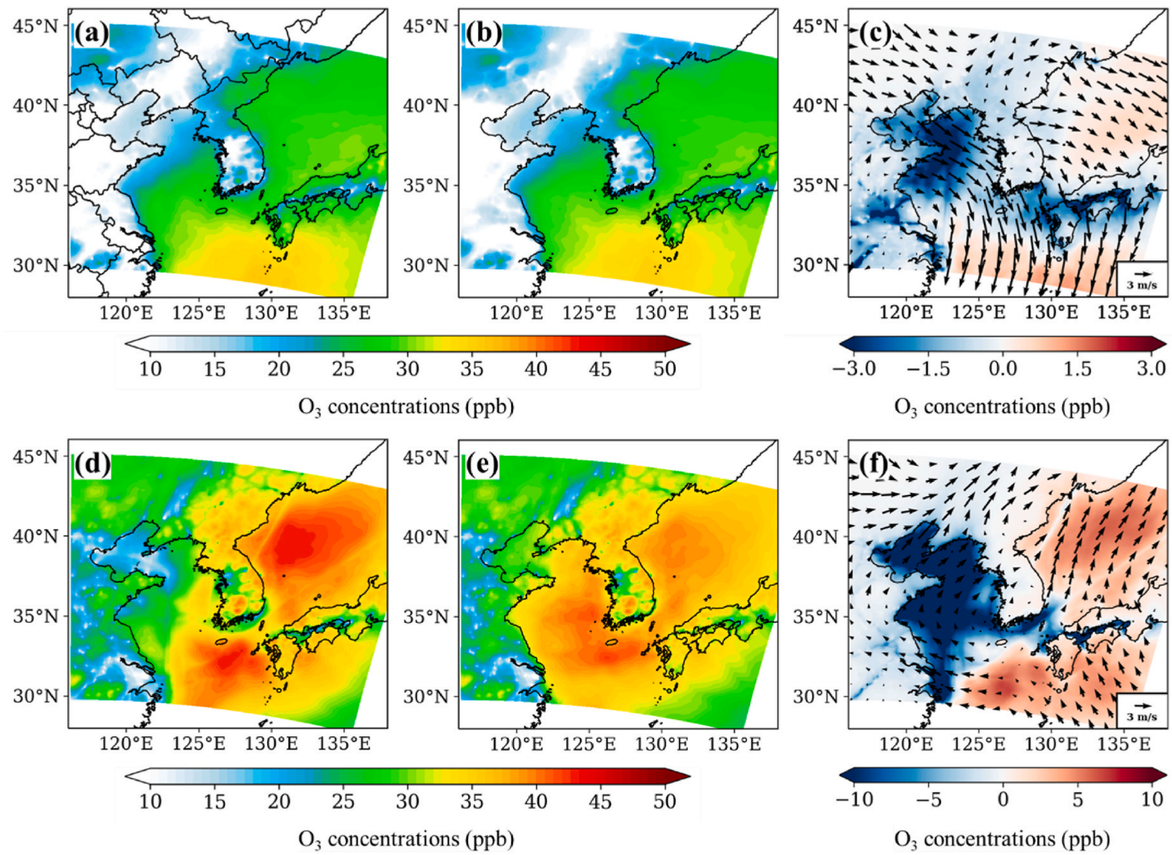

Fig. 5. Horizontal distribution of hourly mean O_3 concentrations for the simulated SIJAQ case ((a), (b), and (c)) and KORUS case ((d), (e), and (f)) during the analysis period. The left panels ((a) and (d)) show the results of the numerical simulations, including shipping emissions, and the results in the middle panels ((b) and (e)) exclude shipping emissions. (c) and (f) represent the O_3 concentrations difference due to shipping emissions for the SIJAQ and KORUS cases, and the averaged wind vector.

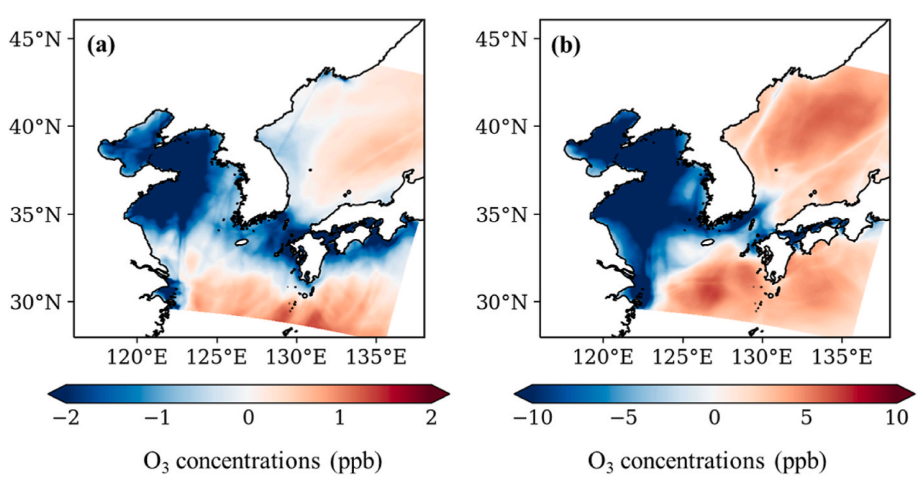

Fig. 6. Spatial distribution of O_3 concentrations changes in the ocean region owing to the difference in shipping emissions in (a) the SIJAQ case and (b) the KORUS case.

located in the Bohai Sea (Dong and Wang, 2012; Wan et al., 2020). Consequently, pollutants such as NO_x emitted from ships navigating through the Bohai Sea and the East China Sea contributed to O_3 decomposition through transportation and dispersion.

3.3. *Differences in O_3 concentrations caused by shipping emissions - ocean area*

The simulation results of the KORUS and SIJAQ cases analyzed earlier were used to analyze the changes in O_3 concentrations caused by shipping emissions. The precursors of O_3 emitted from the ocean can make a greater contribution to the production and destruction reactions of O_3 more than the effects of substances transported from inland. As shown in Fig. S3, the distribution of shipping emissions varies according to region. Therefore, the impact of shipping emissions on O_3 concentrations may also vary according to region.

Fig. 6 shows the distribution of O_3 concentrations changes in ocean areas due to the difference in shipping emissions in the KORUS and

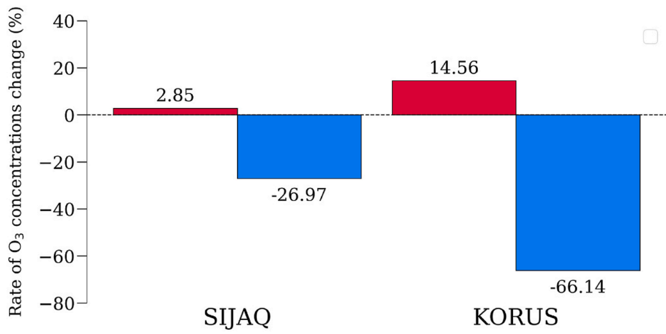

Fig. 7. Boxplot of maximum daily average O_3 concentrations change rate in ocean region due to shipping emissions in the SIJAQ and KORUS cases.

SIJAQ cases (i.e., the case includes shipping emissions minus the case excluding shipping emissions). First, the distribution of O_3 concentrations changes in the SIJAQ case, Fig. 6(a) shows that the difference in shipping emissions resulted in a decrease in O_3 concentrations in parts of the Yellow Sea and East China Sea but an increase in O_3 concentrations in the North Pacific and East Sea. The notable observation here is that despite the increase in emissions, there are areas where O_3 concentrations have decreased. The decrease in O_3 concentrations in those areas is attributed to the decomposition of O_3 by shipping emissions, suggesting that shipping emissions contributed primarily to the O_3 titration reaction rather than O_3 production (Geng et al., 2009; Zhang et al., 2021). Furthermore, the maximum increase in O_3 concentrations in the ocean region was +2.85% (+1.30 ppb), whereas the maximum decrease was −26.97% (8.24 ppb), indicating that more O_3 was decomposed in the ocean region than was produced by shipping emissions (Fig. 7). In other words, in the SIJAQ case, shipping emissions contributed more to the destruction of O_3 in the ocean region than to its production.

For the KORUS case, we examined the change in O_3 concentrations due to the addition of shipping emissions, we found that the distribution of O_3 concentrations was similar to that of the SIJAQ case (Fig. 6(b)). Similar to the SIJAQ case, O_3 concentrations decreased in the Yellow Sea and increased in the North Pacific and East Seas. However, the KORUS case was characterized by a greater influence of shipping emissions than the SIJAQ case, leading to an increase and decrease in O_3 concentration of up to +14.56% (+6.61 ppb) and −66.14% (−28.48 ppb), respectively, in different areas (Fig. 7). The distribution of O_3 concentration differences in both cases is similar, but the variation in the levels of increase and decrease is attributed to the difference in O_3 concentrations between the SIJAQ and KORUS cases, which was identified in Section 3.2. Because of the KORUS case, with higher O_3 concentrations compared to the SIJAQ case, the amount of O_3 decomposition increased, leading to more change in O_3 concentrations attributed to shipping emissions.

The differential impacts of shipping emissions on different regions can be observed in both cases through the O_3 indicator. To analyze the influence of shipping emissions on O_3 concentrations in ocean areas, the H_2O_2/HNO_3 ratio proposed in previous studies was utilized (Sillman, 1995; Li et al., 2011; Shen et al., 2023). Sillman (1995) illustrated that the O_3 sensitivity of a particular region could be classified into a NO_x-sensitive regime and a VOC-sensitive regime based on the H_2O_2/HNO_3 ratio (If a region has $H_2O_2/HNO_3 < 0.35$, it is a VOC-sensitive regime; if $H_2O_2/HNO_3 > 0.60$, it is a NO_x-sensitive regime; if $0.35 < H_2O_2/HNO_3$

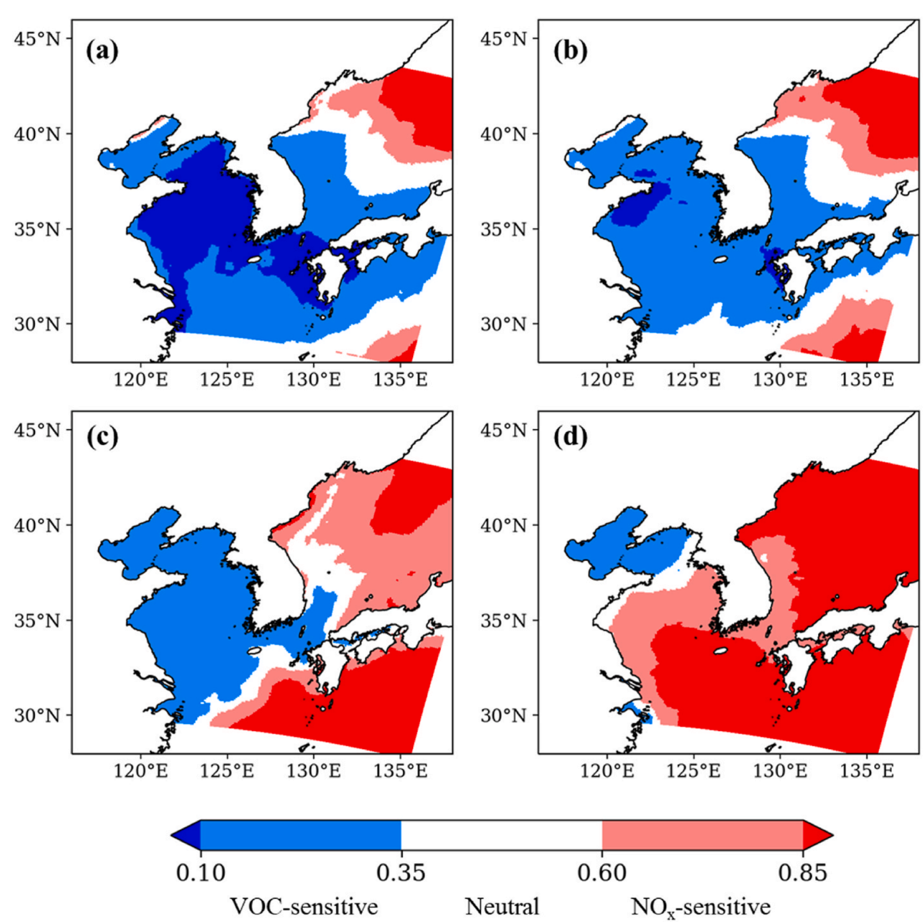

Fig. 8. Spatial distribution of the H_2O_2/HNO_3 ratio in the SIJAQ case ((a) and (b)) and the KORUS case ((c) and (d)). The left panel shows the H_2O_2/HNO_3 ratio in the ocean region, including shipping emissions, and the right panel shows the results excluding shipping emissions.

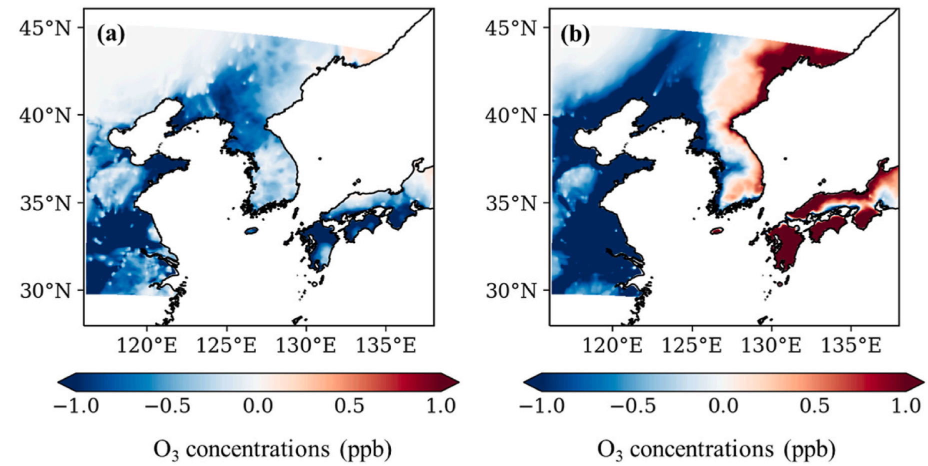

Fig. 9. Spatial distribution of O_3 concentrations changes in inland regions due to differences in shipping emissions in (a) the SIJAQ and (b) the KORUS cases.

< 0.60, it is a NO_x–VOC mixed sensitive regime).

Fig. 8 shows the distribution of the H_2O_2/HNO_3 ratio for the ocean region in the SIJAQ case and the KORUS case, and the distribution of O_3 sensitivity with and without shipping emissions in the SIJAQ case is similar. A comparison of the distribution of O_3 concentrations changes according to shipping emissions in Fig. 6 showed that the regions with decreased O_3 concentrations were distributed in the VOC-sensitive regime, and the regions with increased O_3 concentrations were distributed in the NO_x-sensitive regime (Liu and Shi, 2021). This indicates that shipping emissions can lead to increased O_3 production in areas where O_3 is produced and destroy more O_3 in areas where O_3 is destroyed. As a result, the O_3 indicator analysis shows that NO_x in shipping emissions mainly contributes to O_3 concentrations in ocean areas.

The results of the O_3 indicator analysis in the KORUS case show that O_3 sensitivity changes depending on the presence or absence of shipping emissions. In the Yellow Sea and East China Sea, O_3 sensitivity changed from a NO_x-sensitive regime ($H_2O_2/HNO_3 > 0.60$) in the absence of shipping emissions to a VOC-sensitive regime ($H_2O_2/HNO_3 < 0.35$) as shipping emissions were added, and in some areas of the East Sea, O_3 sensitivity changed from the NO_x-sensitive regime to the NO_x–VOC mixed sensitive regime ($0.35 < H_2O_2/HNO_3 < 0.60$). These regions exhibited a NO_x-sensitive regime in the absence of shipping emissions due to the influence of substances emitted from inland areas transported to the ocean region. However, with the addition of shipping emissions, a large amount of NO_x was emitted into the ocean areas, and the O_3 sensitivity in the regions was consequently changed to the VOC-sensitive regimes.

Therefore, the combined analysis of O_3 concentrations change and sensitivity in the two cases reveals that NO_x in shipping emissions is the main influence on O_3 concentrations in ocean areas when shipping emissions are added. We also found that NO_x from shipping emissions can influence the production and destruction of additional O_3 and change the O_3 sensitivity of ocean areas.

3.4. Differences in O_3 concentrations caused by shipping emissions – land area

Analysis of the change in O_3 concentrations in response to shipping emissions in ocean areas showed that the distribution of the difference in O_3 concentrations was similar in both cases, and the impact of shipping emissions on ocean areas varied according to region. In areas with high NO_x emissions, shipping emissions contributed to O_3 destruction, whereas in areas with low NO_x emissions, they contributed to O_3 production. However, unlike the oceans, inland regions must account for shipping emissions as well as inland emissions, and if shipping emissions are transported inland, inland O_3 concentrations can be altered by complex chemical processes (Khalil, 2018; Lien and Hung, 2021). Therefore, we further analyzed the changes in O_3 concentrations caused by shipping emissions over inland regions.

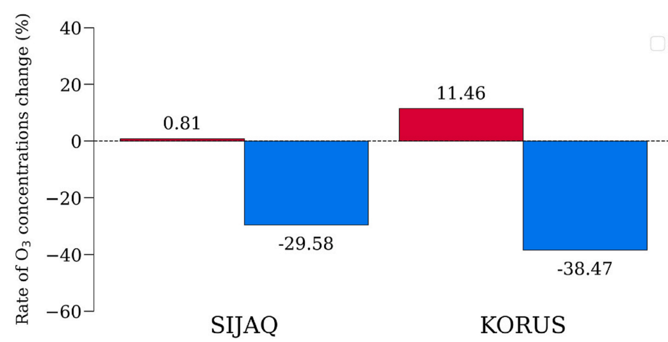

Fig. 10. The same as Fig. 7, but in land area.

Fig. 9(a) shows the distribution of O_3 concentrations changes in inland regions caused by shipping emissions for the SIJAQ case. Most of the regions within the numerical model area, such as eastern China, the Korean Peninsula, and Japan, show a decrease in the O_3 concentration caused by shipping emissions (up to −29.58%, in Fig. 10). As shown in Fig. 2, the inland regions of East Asia, which are predominantly NO_x-rich areas, contribute to the decomposition of already produced O_3 rather than the production of O_3 when shipping emissions are transported inland. This ultimately leads to decreased O_3 concentrations in inland regions caused by shipping emissions. On the other hand, in Manchuria and certain regions of Japan, although O_3 concentrations slightly increased, the increase (up to +0.82%) was very small compared to the amount that decreased. The areas where O_3 increased had significantly lower NO_x emissions than other regions, indicating that shipping emissions contributed to O_3 production rather than O_3 destruction, resulting in increased O_3 concentrations on average. In summary, the changes in inland O_3 concentrations caused by shipping emissions during the SIJAQ case are mainly attributed to the dissipation of O_3 produced by shipping emissions as it is transported inland, similar to the ocean region described in the previous section.

In contrast, the change in O_3 concentrations due to the difference in shipping emissions in the KORUS case showed a different distribution from the SIJAQ case. As shown in Figs. 9(b) and 10, similar to the SIJAQ case, the O_3 concentrations decreased in eastern China up to −38.47% (−16.79 ppb) owing to shipping emissions but increased in the Korean Peninsula and Japan up to +11.46% (+4.79 ppb). The decrease in O_3 concentrations in eastern China is similar to the previous discussion, indicating that shipping emissions primarily contributed to the titration

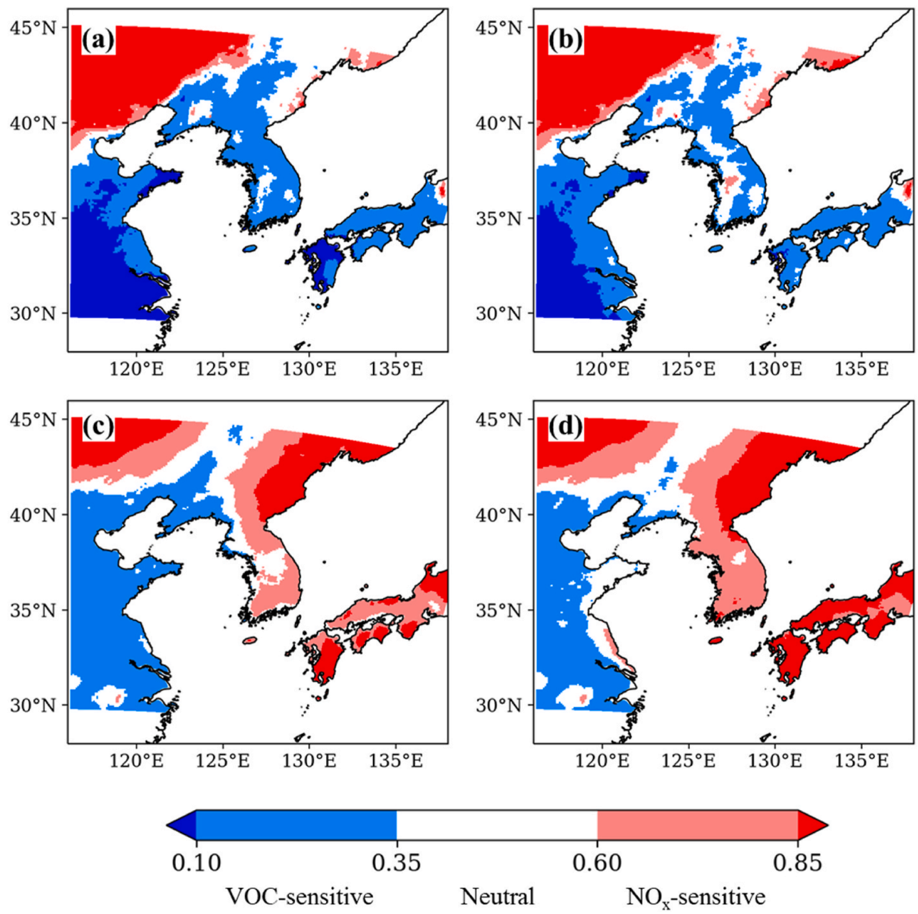

Fig. 11. Spatial distribution of H_2O_2/HNO_3 ratio in the SIJAQ case ((a) and (b)) and KORUS case ((c) and (d)). The left panel shows the H_2O_2/HNO_3 ratio in the inland region, including shipping emissions, and the right panel shows the result without shipping emissions.

reaction of produced O_3. However, in contrast with the SIJAQ case, the Korean Peninsula and Japan in the KORUS case showed a different distribution of O_3 concentrations. This suggests that shipping emissions may not only reduce O_3 concentrations as they are transported inland but, in some cases, could increase O_3 concentrations.

The variation in O_3 concentrations in inland regions according to the different regions can also be explained through the indicators described in the ocean regions. By utilizing the distribution of the H_2O_2/HNO_3 ratio in Fig. 11, the influence of shipping emissions on inland regions was examined. In the case of SIJAQ, H_2O_2/HNO_3 ratios below 0.35 were observed in most regions, indicating a VOC-sensitive regime. This suggests that when NO_x from shipping emissions is transported inland, similar to ocean regions, O_3 can be decomposed through the O_3 titration reactions.

Based on the distribution of the H_2O_2/HNO_3 ratio in the KORUS case, it has been determined that the regions of South Korea and Japan are in the NO_x-sensitive regime with ratios exceeding 0.60, while the eastern region of China belongs to the VOC-sensitive regime with ratios below 0.35. In addition, based on the H_2O_2/HNO_3 ratio distribution in the KORUS case, it is determined that the regions of South Korea and Japan fall into the NO_x-sensitive regime with ratios exceeding 0.60, while the eastern region of China belongs to the VOC-sensitive regime with ratios below 0.35. This means that in the eastern inland regions of China, the transport of NO_x that is already saturated and emitted from ships leads to a decrease in O_3 concentrations. Conversely, in Japan, which is a NO_x-sensitive region, the transport of shipping emissions could increase O_3 concentrations. In the case of the Korean Peninsula, excluding shipping emissions, O_3 sensitivity is predominantly in a NO_x-sensitive regime. However, when shipping emissions are included, the western part of the peninsula changes to a neutral. This indicates that if shipping emissions reach the western part of the Korean Peninsula, there could decrease in O_3 concentrations. Fig. 5(c) shows that the Korean Peninsula is mainly transported by westerly winds, and if shipping emissions from the East China Sea and Yellow Sea are initially transported to the downwind region on the western side of the Korean Peninsula, a significant amount of shipping emissions can contribute to O_3 titration reactions, leading to a decrease in O_3 concentration. Subsequently, shipping emissions were diluted as they were transported from west to east, and the diluted shipping emissions and additional NO_x generated by the O_3 titration reaction in the western part of the Korean Peninsula reacted inland to increase O_3 concentrations. The area of increased O_3 concentrations is where the mountain ranges of the Korean Peninsula are located (e.g. Taebaek and Sobaek mountains, Jung et al., 2007), which have relatively low NO_x emissions, the diluted shipping emissions and the NO_x produced by the O_3 titration reaction were transported to the inland areas of the NO_x-sensitive Korean Peninsula and contributed to O_3 production. Consequently, shipping emissions were transported eastward, they became gradually diluted, contributing more to O_3 production than titration reactions, and O_3 concentrations increased progressively.

We further investigated the effect of BVOC emissions on O_3 production in two cases with different seasons. The difference in growth patterns of trees between the KORUS case, characterized by vigorous leaf growth, and SIJAQ, where leaves fall, showed a significant difference in Leaf Area Index (LAI, Fig. S4), there was a substantial contrast in BVOC emissions between the two cases (Fig. 12). As a result, the O_3 sensitivity of the inland regions of the Korean Peninsula and Japan did not show a distinct difference with or without the inclusion of BVOC

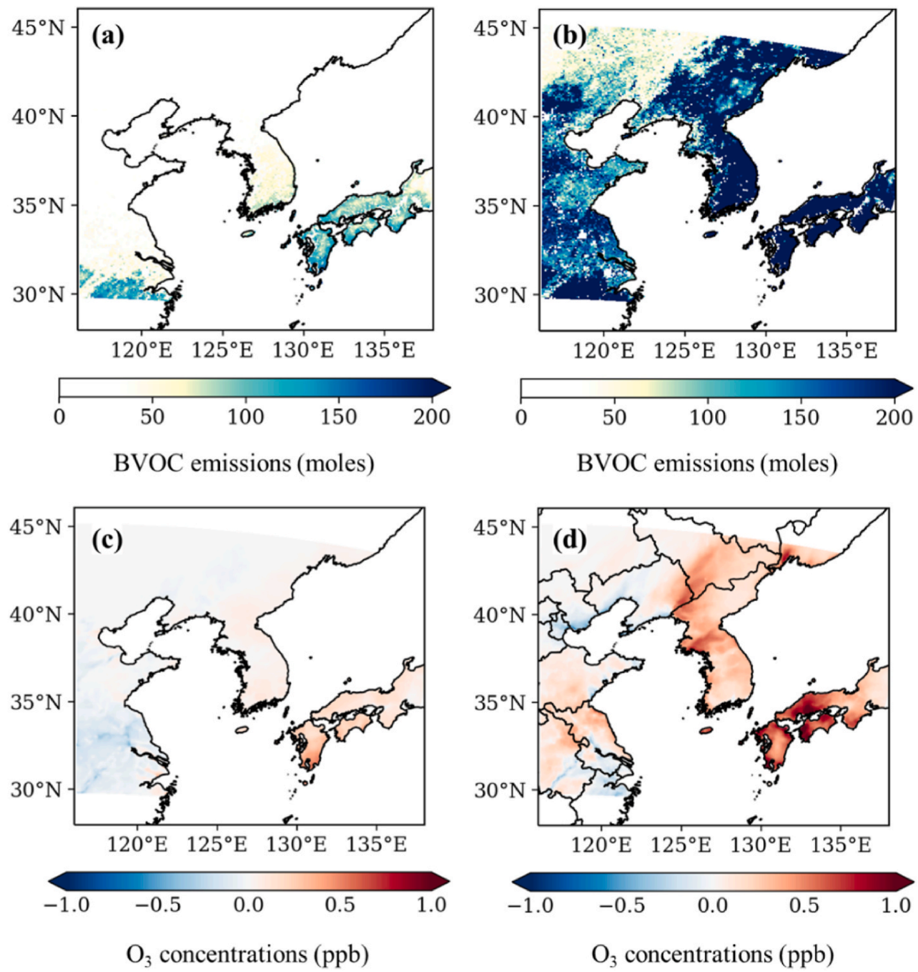

Fig. 12. The spatial distribution of BVOC emissions over the entire simulation period and the difference in O_3 concentrations due to BVOC emissions in the SIJAQ and KORUS cases. Panels (a) and (c) represent the SIJAQ case, while panels (b) and (d) depict the KORUS case.

emissions (Fig. S5). This indicates that BVOC does not play an absolute role in the mechanism of inland O_3 production. However, when BVOC emissions were included, the VOC-sensitive regime in the inland regions of the Korean Peninsula was more extensive, leading to a further increase in O_3 concentrations in the inland regions in the KORUS case, as shown in Fig. 12. These results suggest that the mechanism of O_3 production could be more distinct in inland regions when including BVOC emissions.

4. Summary and conclusion

In this study, we analyzed the impact of shipping emissions on O_3 concentrations during the periods of the KORUS-AQ (the KORUS case) and the SIJAQ 2021 campaign (the SIJAQ case). The CMAQ, a three-dimensional photochemical air quality numerical model, was used to simulate O_3 concentrations, and a case excluding emissions from ocean areas from the EDGARv6.1 data of the anthropogenic emissions used in the simulation was additionally simulated and compared to the case including shipping emissions. The simulation results were verified in three dimensions using ground-based air quality observations, DC-8 observations conducted by KORUS-AQ, and flight observations conducted by the SIJAQ 2021 campaign. The validated results were then used to analyze the impact of shipping emissions on O_3 concentrations.

A comparison between the O_3 concentrations in the two cases simulated by CMAQ showed that the inland O_3 concentrations in the SIJAQ case were lower in South Korea and East China, where NO_x emissions were high. In contrast, Japan and North Korea had relatively high O_3 concentration distributions compared to these regions. The KORUS case showed higher O_3 concentrations compared to the SIJAQ case. Although the emissions in the two cases were similar, O_3 production differed owing to differences in weather conditions (such as high levels of temperature and insolation).

To analyze the impact of shipping emissions in the two cases with different O_3 production, we divided them into ocean and inland regions. First, we analyzed the ocean regions and found that O_3 concentrations decreased in the Yellow Sea and increased in the East Sea and North Pacific caused by shipping emissions, but the amount of increase and decrease in O_3 concentrations was different due to the difference in O_3 production in the two cases. In particular, O_3 concentrations decreased in areas with high shipping emissions, such as the Yellow Sea and the East China Sea, whereas O_3 concentrations increased in regions with low shipping emissions, confirming that differences in emissions can affect O_3 concentrations in ocean regions. Interestingly, the Yellow Sea region was characterized by changing O_3 sensitivity due to ship emissions, when shipping emissions were excluded from the Yellow Sea region, they changed from a NO_x-sensitive regime to a VOC-sensitive regime with the addition of shipping emissions. This suggests that a large amount of shipping emissions from the Yellow Sea region affected the O_3 sensitivity and that shipping emissions contributed to the O_3 titration reaction, which in turn reduced the O_3 concentrations in the ocean region.

Analyzing the changes in O_3 concentrations in inland regions, the SIJAQ case shows a decrease in O_3 concentrations in most parts of East Asia. When checking the O_3 indicator excluding shipping emissions, the

O_3 sensitivity of most inland regions in the SIJAQ case did not change even though shipping emissions were transported to the VOC-sensitive regime, indicating that NO_x in shipping emissions was transported inland and decomposed O_3. In contrast, the KORUS case showed a different concentration distribution inland from the SIJAQ case. In eastern China, O_3 concentrations decreased due to shipping emissions, but interestingly, O_3 concentrations increased in the Korean Peninsula and Japan. Particularly, shipping emissions were predominantly transported to the Korean Peninsula through westerly winds, resulting in an initial decrease in O_3 concentrations in the western regions of the Korean Peninsula. However, during the process of transportation from west to east, the diluted shipping emissions and additional NO_x generated by O_3 titration reactions led to an increase in O_3 concentrations in the relatively low NO_x emission (NO_x-sensitive) inland areas of the Korean Peninsula. Furthermore, examining the influence of BVOC in two cases with different seasons revealed that in the KORUS case with abundant BVOC, the transport of shipping emissions contributed to O_3 production. These findings indicate that ship emissions in the East Asia region primarily decrease O_3 concentrations. However, differences in seasonal and regional O_3 sensitivity and transportation patterns suggest that ship emissions may contribute to O_3 production.

The above results show the impact of shipping emissions on O_3 concentrations in East Asia. Shipping emissions had different effects on the production and destruction of O_3 in inland and ocean regions, and the effects were different in the two cases with different seasons. In particular, the effects of shipping emissions on O_3 production and destruction were quantitatively different, owing to differences in weather conditions in the two cases with different seasons. The results confirm that shipping emissions can produce O_3 when transported inland in the NO_x-rich East Asian region, thereby elucidating the O_3 formation process in the region.

However, because this study analyzed the impact of shipping emissions on O_3 concentrations in a limited number of regions and cases, and in the SIJAQ case, emissions for the current year were not available, the impact of COVID-19 could not be considered. Nevertheless, further research on various cases and regions based on this study is expected to elucidate and clarify the impact of shipping emissions on O_3 concentrations.

CRediT authorship contribution statement

Jaehyeong Park: Conceptualization, Formal analysis, Methodology, Writing – original draft. **Jeonghyeok Mun:** Formal analysis, Software, Visualization. **Dongjin Kim:** Formal analysis, Investigation, Validation. **Hwa Woon Lee:** Supervision. **Cheol-Hee Kim:** Conceptualization, Funding acquisition. **Hyo-Jung Lee:** Formal analysis, Investigation. **Hyun-Young Jo:** Formal analysis, Visualization. **Ja-Yong Koo:** Formal analysis, Funding acquisition. **Hyeonsik Choe:** Investigation, Validation. **Wonbae Jeon:** Conceptualization, Methodology, Project administration, Supervision, Writing – review & editing.

Declaration of competing interest

The authors declare that they have no known competing financial interests or personal relationships that could have appeared to influence the work reported in this paper.

Data availability

Data will be made available on request.

Acknowledgements

This research was partially supported by the Basic Science Research Program through the National Research Foundation of Korea (NRF) funded by the Ministry of Education (NRF-2020R1A6A1A03044834) and the National Research Foundation of Korea (NRF) grant funded by the Korea government (MSIT) (No. 2023R1A2C1002608).

Appendix A. Supplementary data

Supplementary data to this article can be found online at https://doi.org/10.1016/j.atmosenv.2024.120339.

References

Akimoto, H., Mori, Y., Sasaki, K., Nakanishi, H., Ohizumi, T., Itano, Y., 2015. Analysis of monitoring data of ground-level ozone in Japan for long-term trend during 1990–2010: causes of temporal and spatial variation. Atmos. Environ. 102, 302–310. https://doi.org/10.1016/j.atmosenv.2014.12.001.

Appel, K.W., Bash, J.O., Fahey, K.M., Foley, K.M., Gilliam, R.C., Hogrefe, C., Hutzell, W. T., Kang, D., Mathur, R., Murphy, B.N., Napelenok, S.L., Nolte, C.G., Pleim, J.E., Pouliot, G.A., Pye, H.O.T., Ran, L., Roselle, S.J., Sarwar, G., Schwede, D.B., Sidi, F.I., Spero, T.L., Wong, D.C., 2021. The Community Multiscale Air Quality (CMAQ) model versions 5.3 and 5.3.1: system updates and evaluation. Geosci. Model Dev. (GMD) 14, 2867–2897. https://doi.org/10.5194/gmd-14-2867-2021.

Calfapietra, C., Pallozzi, E., Lusini, I., Velikova, V., 2013. Modification of bvoc emissions by changes in atmospheric [CO2] and air pollution. In: Niinemets, Ü., Monson, K.R. (Eds.), Biology, Controls and Models of Tree Volatile Organic Compound Emissions. Springer Netherlands, Dordrecht, pp. 253–284.

Chang, K., Petropavlovskikh, I., Cooper, O., Schultz, M., Wang, T., 2017. Regional trend analysis of surface ozone observations from monitoring networks in eastern North America, Europe and East Asia. Elementa 5, 1–22. https://doi.org/10.1525/elementa.243.

Ching, J., Byun, D., 1999. Introduction to the Models-3 Framework and the Community Multiscale Air Quality Model (CMAQ), Science Algorithms of the EPA Models-3 Community Multiscale Air Quality (CMAQ) Modeling System.

Choi, J., Park, R.J., Lee, H.-M., Lee, S., Jo, D.S., Jeong, J.I., Henze, D.K., Woo, J.-H., Ban, S.-J., Lee, M.-D., Lim, C.-S., Park, M.-K., Shin, H.J., Cho, S., Peterson, D., Song, C.-K., 2019. Impacts of local vs. trans-boundary emissions from different sectors on $PM_{2.5}$ exposure in South Korea during the KORUS-AQ campaign. Atmos. Environ. 203, 196–205. https://doi.org/10.1016/j.atmosenv.2019.02.008.

Crawford, J.H., Ahn, J.Y., Al-Saadi, J., Chang, L., Emmons, L.K., Kim, J., Lee, G., Park, J. H., Park, R.J., Woo, J.H., Chang-Keun Song, C.-K., Hong, J.-H., Hong, Y.-.D., Lefer, B. L., Lee, M., Lee, T., Kim, S., Min, K.-E., Yum, S.S., Shin, H.J., Kim, Y.-W., Choi, J.-S., Park, J.-S., Szykman, J.J., Long, R.W., Jordan, C.E., Simpson, I.J., Fried, A., Dibb, J. E., Cho, S.Y., Kim, Y.P., 2021. The Korea–United States air quality (KORUS-AQ) field study. Elem. Sci. Anth. 9 (1), 00163 https://doi.org/10.1525/elementa.2020.00163.

Crippa, M., Guizzardi, D., Muntean, M., Schaaf, E., Monforti-Ferrario, F., Banja, M., Pagani, F., Solazzo, E., 2022. EDGAR v6.1 Global Air Pollutant Emissions. European Commission, Joint Research Centre (JRC). http://data.europa.eu/89h/df521e05-6a3b-461c-965a-b703fb62313e.

Dong, X., Wang, G., 2012. Coal logistics competency strategies for ports in the Tianjin and Hebei regions around the Bohai Bay in China. Energy Proc. 17, 436–443. https://doi.org/10.1016/j.egypro.2012.02.117.

Ducruet, C., Lee, S.-W., Ng, A.K.Y., 2010. Centrality and vulnerability in liner shipping networks: revisiting the Northeast Asian port hierarchy. Marit. Pol. Manag. 37 (1), 17–36. https://doi.org/10.1080/03088830903461175.

Emery, C., Liu, Z., Russell, A.G., Odman, M.T., Yarwood, G., Kumar, N., 2017. Recommendations on statistics and benchmarks to assess photochemical model performance. J. Air Waste Manag. Assoc. 67 (5), 582–598. https://doi.org/10.1080/10962247.2016.1265027.

European Environment Agency (EEA), European Oean Safety Agency (EMSA), 2021. European Ocean Transport Environmental Report 2021. Publications Office of the European Union. https://data.europa.eu/doi/10.2800/3525.

Fu, Y., Li, R., Hu, J., Wang, Y., Duan, J., 2022. Investigating the impacts of satellite fire observation accuracy on the top-down nitrogen oxides emission estimation in northeastern Asia. Environ. Int. 169, 107498 https://doi.org/10.1016/j.envint.2022.107498.

Geng, F.H., Zhang, Q., Tie, X., Huang, M., Ma, X., Deng, Z., Yu, Q., Quan, J., Zhao, C., 2009. Aircraft measurements of O_3, NO_x, CO, VOCs, and SO_2 in the yangtze river delta region. Atmos. Environ. 43, 584–593. https://doi.org/10.1016/j.atmosenv.2008.10.021.

Griffith, S.M., Huang, W.S., Lin, C.C., Chen, Y.C., Chang, K.E., Lin, T.H., Wang, S.H., Lin, N.H., 2020. Long-range air pollution transport in East Asia during the first week of the COVID-19 lockdown in China. Sci. Total Environ. 741, 140214 https://doi.org/10.1016/j.scitotenv.2020.140214.

Guenther, A.B., Jiang, X., Heald, C.L., Sakulyanontvittaya, T., Duhl, T., Emmons, L.K., Wang, X., 2012. The model of emissions of gases and aerosols from nature version 2.1 (MEGAN2.1): an extended and updated framework for modeling biogenic emissions. Geosci. Model Dev. (GMD) 5, 1471–1492. https://doi.org/10.5194/gmd-5-1471-2012.

Hurley, P.J., Blockley, A., Rayner, K., 2001. Verification of a prognostic meteorological and air pollution model for year-long predictions in the Kwinana industrial region of Western Australia. Atmos. Environ. 35 (10), 1871–1880. https://doi.org/10.1016/S1352-2310(00)00486-6.

Itahashi, S., Irie, H., Shimadera, H., Chatani, S., 2022. Fifteen-year trends (2005–2019) in the satellite-derived ozone-sensitive regime in East Asia: a gradual shift from VOC-

sensitive to NO_x-sensitive. Rem. Sens. 14 (18), 4512. https://doi.org/10.3390/rs14184512.
Jeon, W., Choi, Y., Lee, H.W., Lee, S.H., Yoo, J.W., Park, J., Lee, H.J., 2015. A quantitative analysis of grid nudging effect on each process of $PM_{2.5}$ production in the Korean Peninsula. Atmos. Environ. 122, 763–774. https://doi.org/10.1016/j.atmosenv.2015.10.050.
Jiménez, P., Parra, R., Gassó, S., Baldasano, J.M., 2005. Modeling the ozone weekend effect in very complex terrains: a case study in the Northeastern Iberian Peninsula. Atmos. Environ. 39 (3), 429–444. https://doi.org/10.1016/j.atmosenv.2004.09.065.
Jung, J., Choi, Y., Souri, A.H., Mousavinezhad, S., Sayeed, A., Lee, K., 2022. The impact of springtime-transported air pollutants on local air quality with satellite-constrained NO_x emission adjustments over East Asia. J. Geophys. Res. Atmos. 127, e2021JD035251 https://doi.org/10.1029/2021JD035251.
Jung, J., Jung, Y., Min, G.S., Kim, W., 2007. Analysis of the population genetic structure of the malaria vector *Anopheles sinensis* in South Korea based on mitochondrial sequences. Am. J. Trop. Med. Hyg. 77, 310–315. https://doi.org/10.4269/ajtmh.2007.77.310.
Khalil, M.A.K., 2018. Steady states and transport processes in urban ozone balances. NPJ Clim. Atmos. Sci. 1, 22. https://doi.org/10.1038/s41612-018-0035-7.
Kim, D., Jeon, W., Park, J., Mun, J., Choi, H., Kim, C.H., Lee, H.J., Jo, H.Y., 2022. A numerical analysis of the changes in O_3 concentrations in a wildfire plume. Rem. Sens. 14 (18), 4549. https://doi.org/10.3390/rs14184549.
Kim, J., Ghim, Y.S., Han, J.-S., Park, S.-M., Shin, H.-J., Lee, S.-B., Kim, J., Lee, G., 2018. Long-term trend analysis of Korean air quality and its implication to current air quality policy on ozone and PM_{10}. J. Korean Soc. Atmos. Environ. 34 (1), 1–15. https://doi.org/10.5572/kosae.2018.34.1.001.
LeBlanc, S.E., Segal-Rozenhaimer, M., Redemann, J., Flynn, C., Johnson, R.R., Dunagan, S.E., Dahlgren, R., Kim, J., Choi, M., da Silva, A., Castellanos, P., Tan, Q., Ziemba, L., Lee Thornhill, K., Kacenelenbogen, M., 2022. Airborne observations during KORUS-AQ show that aerosol optical depths are more spatially self-consistent than aerosol intensive properties. Atmos. Chem. Phys. 22, 11275–11304. https://doi.org/10.5194/acp-22-11275-2022.
Lee, J., Woo, J., 2020. Green new deal policy of South Korea: policy innovation for a sustainability transition. Sustainability 12 (23), 10191. https://doi.org/10.3390/su122310191.
Lee, G., Park, J.H., Kim, D.G., Koh, M.S., Lee, M., Han, J.S., Kim, J.C., 2020. Current status and future directions of tropospheric photochemical ozone studies in Korea. J. Korean Soc. Atmos. Environ. 36 (4), 419–441. https://doi.org/10.5572/KOSAE.2020.36.4.419.
Lee, H., Jo, H., Park, S., Jo, Y., Jeon, W., Ahn, J., Kim, C., 2019. A case study of the transport/transformation of air pollutants over the Yellow Sea during the MAPS 2015 campaign. J. Geophys. Res. Atmos. 124, 6532–6553. https://doi.org/10.1029/2018JD029751.
Lee, H., Chang, L., Jaffe, D.A., Bak, J., Liu, X., Abad, G.G., Jo, H., Jo, Y., Lee, J., Yang, G., Kim, J., Kim, C., 2022. Satellite-based diagnosis and numerical verification of ozone formation regimes over nine megacities in East Asia. Rem. Sens. 14 (5), 1285. https://doi.org/10.3390/rs14051285.
Li, L., Chen, C., Huang, C., Huang, H., Zhang, G., Wang, Y., Chen, M., Wang, H., Chen, Y., Streets, D.G., Fu, J., 2011. Ozone sensitivity analysis with the MM5-CMAQ modeling system for Shanghai. J. Environ. Sci. 23 (7), 1150–1157. https://doi.org/10.1016/S1001-0742(10)60527-X.
Li, Z., Lau, W.K., Ramanathan, V., Wu, G., Ding, Y., Manoj, M.G., Liu, J., Qian, Y., Li, J., Zhou, T., Fan, J., Rosenfeld, D., Ming, Y., Wang, Y., Huang, J., Wang, B., Xu, X., Lee, S., Cribb, M., Zhang, F., Yang, X., Zhao, C., Takemura, T., Wang, K., Xia, X., Yin, Y., Zhang, H., Guo, J., Zhai, P.M., Sugimoto, N., Babu, S.S., Brasseur, G.P., 2016. Aerosol and monsoon climate interactions over Asia. Rev. Geophys. 54, 866–929. https://doi.org/10.1002/2015RG000500.
Lien, J., Hung, H.M., 2021. The contribution of transport and chemical processes on coastal ozone and emission control strategies to reduce ozone. Heliyon 7, e08210. https://doi.org/10.1016/j.heliyon.2021.e08210.
Lin, B., Zhu, J., 2019. Impact of energy saving and emission reduction policy on urban sustainable development: empirical evidence from China. Appl. Energy 239 (1), 12–22. https://doi.org/10.1016/j.apenergy.2019.01.166.
Liu, C.Q., Shi, K., 2021. A review on methodology in O_3-NO_x-VOC sensitivity study. Environ. Pollut. 291, 118249 https://doi.org/10.1016/j.envpol.2021.118249.
Liu, Y., Li, L., An, J., Huang, L., Yan, R., Huang, C., Wang, H., Wang, Q., Wang, M., Zhang, W., 2018. Estimation of biogenic VOC emissions and its impact on ozone formation over the Yangtze River Delta region, China. Atmos. Environ. 186, 113–128. https://doi.org/10.1016/j.atmosenv.2018.05.027.
Luo, W., Kim, H.S., Zhao, X., Ryu, D., Jung, I., Cho, H., Harris, N., Ghosh, S., Zhang, C., Liang, J., 2020. New forest biomass carbon stock estimates in Northeast Asia based on multisource data. Global Change Biol. 26 (12), 7045–7066. https://doi.org/10.1111/gcb.15376.
Morisada, K., Ono, K., Kanomata, H., 2004. Organic carbon stock in forest soils in Japan. Geoderma 119 (1–2), 21–32. https://doi.org/10.1016/S0016-7061(03)00220-9.
Mun, J., Choi, Y., Jeon, W., Lee, H.W., Kim, C., Park, S., Bak, J., Jung, J., Oh, I., Park, J., Kim, D., 2023. Assessing mass balance-based inverse modeling methods via a pseudo-observation test to constrain NO_x emissions over South Korea. Atmos. Environ. 292, 119429 https://doi.org/10.1016/j.atmosenv.2022.119429.
Oh, S.U., Park, S.Y., 2023. Implications of North Korean forest policy and "golden mountain strategy.". Pacific Focus 38 (1), 105–126. https://doi.org/10.1111/pafo.12222.
Paraschiv, S., Barbuta-Misu, N., Paraschiv, S.L., 2020. Influence of NO_2, NO and meteorological conditions on the tropospheric O_3 concentration at an industrial station. Energy Rep. 6, 231–236. https://doi.org/10.1016/j.egyr.2020.11.263.
Park, M., Yum, S.S., Kim, N., Anderson, B.E., Beyersdorf, A., Thornhill, K.L., 2020. On the submicron aerosol distributions and CCN activity in and around the Korean Peninsula measured onboard the NASA DC-8 research aircraft during the KORUS-AQ field campaign. Atmos. Res. 243, 105004 https://doi.org/10.1016/j.atmosres.2020.105004.
Peterson, D.A., Hyer, E.J., Han, S., Crawford, J.H., Park, R.J., Holz, R., Kuehn, R.E., Eloranta, E., Knote, C., Jordan, C.E., Lefer, B.L., 2019. Meteorology influencing springtime air quality, pollution transport, and visibility in Korea. Elementa 7, 57. https://doi.org/10.1525/elementa.395.
Qi, R., Shi, C., Wang, M.Y., 2022. Carbon emission rush in response to the carbon reduction policy in China. China Inf. 37 (1), 100–122. https://doi.org/10.1177/0920203X221093188.
Shimadera, H., Hayami, H., Morino, Y., Ohara, T., Chatani, S., Hasegawa, S., Kaneyasu, N., 2013. Analysis of summertime atmospheric transport of fine particulate matter in northeast Asia. Asia-Pacific J. Atmos. Sci. 49, 347–360. https://doi.org/10.1007/s13143-013-0033-y.
Sillman, S., 1995. The use of NO_y, H_2O_2, and HNO_3 as indicators for ozone-NO_x-hydrocarbon sensitivity in urban locations. J. Geophys. Res. Atmos. 100 (D7), 14175–14188. https://doi.org/10.1029/94JD02953.
Singh, M., Singh, B.B., Singh, R., Upendra, B., Kaur, R., Gill, S.S., Biswas, M.S., 2021. Quantifying COVID-19 enforced global changes in atmospheric pollutants using cloud computing based remote sensing. Remote Sens. Appl.: Soc. Environ. 22 https://doi.org/10.1016/j.rsase.2021.100489.
Skamarock, W.C., Klemp, J.B., Dudhia, J., Gill, D.O., Barker, D.M., Duda, M.G., Huang, X., Wang, W., Powers, J.G., 2019. A description of the Advanced Research WRF version 4. In: NCAR Technical Note, Mesoscale and Microscale Meteorology Laboratory National Center for Atmospheric Research. https://doi.org/10.6084/m9.Figshare.7369994.v4.
Song, A., Yan, Y., Kong, S., Ma, J., Tong, Z., 2022. Impact of synoptic climate system interaction on surface ozone in China during 1950–2014. Atmos. Environ. 279, 119126 https://doi.org/10.1016/j.atmosenv.2022.119126.
Song, B., Park, K., 2021. Temperature trend analysis associated with land-cover changes using time-series data (1980-2019) from 38 weather stations in South Korea. Sustain. Cities Soc. 65, 102615 https://doi.org/10.1016/j.scs.2020.102615.
Stauffer, D.R., Seaman, N.L., 1990. Use of four-dimensional data assimilation in a limited-area mesoscale model. Part I: experiments with synoptic-scale data. Mon. Weather Rev. 118 (6), 1250–1277. https://doi.org/10.1175/1520-0493(1990)118<1250:UOFDDA>2.0.CO;2.
Sugiyama, M., Fujimori, S., Wada, K., Endo, S., Fujii, Y., Komiyama, R., Kato, E., Kurosawa, A., Matsuo, Y., Oshiro, K., Fumimori, S., Shiraki, H., 2019. Japan's long-term climate mitigation policy: multi-model assessment and sectoral challenges. Energy 167, 1120–1131. https://doi.org/10.1016/j.energy.2018.10.091.
Takahashi, M., Feng, Z., Mikhailova, T.A., Kalugina, O.V., Shergina, O.V., Afanasieva, L. V., Heng, R.K.J., Majid, N.M.N.A., Sase, H., 2020. Air pollution monitoring and tree and forest decline in East Asia: a review. Sci. Total Environ. 742, 140288 https://doi.org/10.1016/J.SCITOTENV.2020.140288.
UNCTAD, 2022. Review of Ocean Transport 2022. United Nations. https://unctad.org/system/files/official-document/rmt2022_en.pdf. (Accessed 18 March 2023).
Uranishi, K., Ikemori, F., Shimadera, H., Kondo, A., Sugata, S., 2019. Impact of field biomass burning on local pollution and long-range transport of $PM_{2.5}$ in Northeast Asia. Environ. Pollut. 244, 414–422. https://doi.org/10.1016/j.envpol.2018.09.061.
Vincent, C.L., Hahmann, A.N., 2015. The impact of grid and spectral nudging on the variance of the near-surface wind speed. J. Appl. Meteorol. Climatol. 54, 1021–1038. https://doi.org/10.1175/JAMC-D-14-0047.1.
Vogel, B., Günther, G., Müller, R., Grooß, J., Afchine, A., Bozem, H., Hoor, P., Krämer, M., Müller, S., Riese, M., Rolf, C., Spelten, N., Stiller, G.P., Ungermann, J., Zahn, A., 2016. Long-range transport pathways of tropospheric source gases originating in Asia into the northern lower stratosphere during the Asian monsoon season 2012. Atmos. Chem. Phys. 16, 15301–15325. https://doi.org/10.5194/acp-16-15301-2016.
Wan, Z., Ji, S., Liu, Y., Zhang, Q., Chen, J., Wang, Q., 2020. Shipping emission inventories in China's Bohai bay, yangtze river delta, and pearl river delta in 2018. Mar. Pollut. Bull. 151, 110882 https://doi.org/10.1016/j.marpolbul.2019.110882.
Wang, J., Xu, J., He, Y., Chen, Y., Meng, F., 2016. Long range transport of nitrate in the low atmosphere over Northeast Asia. Atmos. Environ. 144, 315–324. https://doi.org/10.1016/j.atmosenv.2016.08.084.
Wang, J., Yang, Y., Zhang, Y., Niu, T., Jiang, X., Wang, Y., Che, H., 2019. Influence of meteorological conditions on explosive increase in O_3 concentration in troposphere. Sci. Total Environ. 652, 1228–1241. https://doi.org/10.1016/j.scitotenv.2018.10.228.
Wang, S.X., Zhao, B., Cai, S.Y., Klimont, Z., Nielsen, C.P., Morikawa, T., Woo, J.H., Kim, Y., Fu, X., Xu, J.Y., Hao, J.M., He, K.B., 2014. Emission trends and mitigation options for air pollutants in East Asia. Atmos. Chem. Phys. 14 (13), 6571–6603. https://doi.org/10.5194/acp-14-6571-2014.
Wang, T., Dai, J., Lam, K.S., Nan Poon, C., Brasseur, G.P., 2019. Twenty-five years of lower tropospheric ozone observations in tropical East Asia: the influence of emissions and weather patterns. Geophys. Res. Lett. 46, 11463–11470. https://doi.org/10.1029/2019GL084459.
Wang, X., Liang, X., Jiang, W., Tao, Z., Wang, J.X.L., Liu, H., Han, Z., Liu, S., Zhang, Y., Grell, G.A., Peckham, S.E., 2010. WRF-Chem simulation of East Asian air quality: sensitivity to temporal and vertical emissions distributions. Atmos. Environ. 44, 660–669. https://doi.org/10.1016/j.atmosenv.2009.11.011.
Willmott, C.J., Ackleson, S.G., Davis, R.E., Feddema, J.J., Klink, K.M., Legates, D.R., O'donnell, J., Rowe, C.M., 1985. Statistics for the evaluation and comparison of models. J. Geophys. Res. 90 (C5), 8995–9005. https://doi.org/10.1029/JC090iC05p08995.

Xu, Z., Yao, L., Liu, Q., Long, Y., 2019. Policy implications for achieving the carbon emission reduction target by 2030 in Japan-Analysis based on a bilevel equilibrium model. Energy Pol. 134, 110939 https://doi.org/10.1016/j.enpol.2019.110939.
Zhang, X., Fung, J.C.H., Lau, A.K.H., Hossain, M.S., Louie, P.K.K., Huang, W., 2021. Air quality and synergistic health effects of ozone and nitrogen oxides in response to China's integrated air quality control policies during 2015–2019. Chemosphere 268, 129385. https://doi.org/10.1016/j.chemosphere.2020.129385.
Zhao, H., Wang, S., Wang, W., Liu, R., Zhou, B., 2015. Investigation of ground-level ozone and high-pollution episodes in a megacity of Eastern China. PLoS One 10 (6), e0131878. https://doi.org/10.1371/journal.pone.0131878.